Electronic Supplementary Material (ESI) for Energy & Environmental Science.

Supporting Information

Quantifying lithium concentration gradients in the graphite electrode of Li-ion cells using *operando* energy dispersive X-ray diffraction

Koffi P.C. Yao, [1] John S. Okasinski, [2] Kaushik Kalaga, [1] Ilya A. Shkrob, [1] and Daniel P. Abraham* [1]

[1] Chemical Sciences and Engineering Division, Argonne National Laboratory, 9700 Cass Avenue, Argonne, Illinois 60439, USA

[2] Advanced Photon Source, Argonne National Laboratory, 9700 Cass Avenue, Argonne, Illinois 60439, USA

* Corresponding author: E-mail: abraham@anl.gov

List of abbreviations

CE	Coulombic efficiency
EDXRD	Energy dispersive X-ray diffraction
Gr	graphite
LIB	lithium ion battery
NCM*xyz*	layered lithiated nickel-cobalt-manganese oxide (x+y+z=10)
PVdF	polyvinylidene fluoride (polymer binder in microporous electrodes)
PE	polyethylene
PP	polypropylene
SEI	solid electrolyte interphase
SOC	state of charge
XRD	X-ray diffraction

Section S1. XRD probing.

The beam profile in the transverse direction z is given by a normalized function $g(z)$ with the centroid placed at z=0, so that

$$\int_{-\infty}^{+\infty} dz\, g(z) = 1 \qquad \text{(S1)}$$

$$\int_{-\infty}^{+\infty} dz\, z g(z) = 0 \qquad \text{(S2)}$$

This function was determined experimentally using the digitized X-ray radiographs shown in Figure 1. The experimental beam profile $g(z)$ approximately corresponds to a Gaussian $exp(-[z/\sigma]^2)/\sigma\sqrt{\pi}$ with $\sigma \approx 11.0 \pm 0.3$ μm, which corresponds to 18.3 mm fwhm. For each true beam position $z = z_0$, which is known from the absolute motor position of the cell, the centroid z_1 of the probed volume was calculated as

$$z_1 = \int_0^L dz\, z\, g(z - z_0) \Big/ \int_0^L dz\, g(z - z_0) \qquad \text{(S3)}$$

where L=114 μm is the electrode thickness. The corresponding true positions z_0 and centroids z_1 are summarized below

Layer	z_0 μm	z_1 μm
L_0	4	8.03
L_1	29	29.0
L_2	54	54.0
L_3	79	79.0
L_4	104	102.6

These centroids are given as the effective layer depths in the tables and plots. For a concentration profile $c(z)$, the layer average $C(z_1)$ for a beam centered at z_0 is given by

$$C(z_1) = \int_0^L dz\, c(z)\, g(z - z_0) \Big/ \int_0^L dz\, g(z - z_0) \qquad \text{(S4)}$$

This quantity can be calculated for any trial $c(z)$ and compared with our experimental observables. The normalization in eq. S4 takes into account the geometric overlap of the X-ray beam with the graphite matrix shown in Figure 1, but it does not take into account matrix porosity. We remind that lithium concentrations calculated in section S2 are given *per unit C_6 cell of graphite* as opposed to the volume, so these quantities already take into account pores in the matrix (and any inhomogeneity resulting from porosity gradients). We emphasize that unless $c(z)$ is constant (i.e.,

there is no concentration gradient) there is no *a priori* reason to expect that the average of $C(z_1)$ corresponds to the volume average $\bar{c}$ of $c(z)$, which is given by

$$\bar{c} = \frac{1}{L}\int_0^L dz\, c(z)$$

To produce plots shown in Figure 9, we assumed that for $c'(0) < 0$

$$c(z) \approx A\, e^{-az} + Be^{-bz} + C, \qquad \text{(S5)}$$

so that $c'(0) \approx -Aa - Bb$, whereas for $c'(0) > 0$ we assumed the polynomial expression

$$c(z) \approx \sum_{m=0}^{4} a_m z^m \qquad \text{(S6)}$$

and $c'(0) \approx a_1$. The coefficients in eqs. S5 and S6 were determined using the nonlinear least squares minimization of deviations between the experimental and theoretical $C(z_1)$ calculated using eq. S4 with the experimental $g(z)$ for each layer. Figure 9 in the text shows the resulting profiles $c(z)$.

Section S2. Derivation of Eq. 1.

Let $f_j = 1/y$ be the fractional Li content per C_6 of the ordered LiC_{6y} phase j (y=1-5 in Table S2), I_j be the relative integrated flux of scattered X-ray photons from this phase, m_j be the multiplicity of the Bragg reflection originating from this phase in the peak region of interest, and F_j be the corresponding scattering factor (see Table S2 for estimates of these parameters for specific LiC_{6y} phases). The scattering intensity I_j for each phase j is given by

$$I_j = \alpha\, m_j \cdot |F_j|^2\, N_j,$$

where N_j is the number of unit cells in the probed volume and α is the (unknown) proportionality coefficient that is the same for each phase j. Since each LiC_{6y} cell contains one lithium atom and f_j^{-1} C_6 units, the number of lithium atoms contained in the LiC_{6y} phases in the probed volume is given by

$$[Li]_j = \frac{I_j}{\alpha\, m_j \cdot |F_j|^2} = \frac{\Gamma_j}{\alpha} \qquad \text{(S7)}$$

whereas the number of C_6 units in the same volume is given by

$$[C_6]_j = \frac{\Gamma_j}{\alpha\, f_j} \qquad \text{(S8)}$$

The sum of individual contributions in eq. S8

$$[C_6]_{total} = \sum_j \frac{\Gamma_j}{\alpha f_j} \tag{S9}$$

gives the total number $[C_6]_{total}$ of the C_6 units in the probed volume, whereas the sum of contributions given by eq. S7 adds to the total number of Li atoms in the same volume. This allows exclusion of α, obtaining

$$x_j = \Gamma_j \Big/ \sum_j f_j^{-1} \Gamma_j \tag{S10}$$

and

$$x = \sum_j x_j \tag{S11}$$

where x is the average Li content (over all phases) and x_j are individual contributions to this average from each LiC_{6y} phase in the probed volume. As the theoretical capacity is calculated assuming one Li atom per C_6 atoms of graphite, these expressions also give the lithiation extents. The total concentration of C_6 units in eq. S9 is also given by

$$[C_6]_{total} = \frac{\Gamma_{Gr}}{\alpha} \tag{S12}$$

where Gr pertains to X-rays scattered by graphite before the matrix becomes lithiated (as the same number of graphite cells is present before and after the lithiation). We used the latter expression in all data processing. The advantage of normalization using eq. S10 is that it excludes shot noise, whereas using eq. S12 minimizes possible effects due to errors in the scattering factors (as the graphite values are the most accurate), but introduces shot noise. Note that only ordered LiC_{6y} phases are considered in this derivation.

The equivalence of eqs. S9 and S12 gives a convenient internal check on the consistency of scattering factors in eq. S7, as this equivalence can be rewritten as

$$1 = \sum_j \beta_j u_{j\mu} \quad , \tag{S13}$$

where we defined

$$u_{j\mu} = \frac{I_j^\mu}{f_j m_j} \Big/ \frac{I_{Gr}}{f_{Gr} m_{Gr}} , \tag{S14}$$

$$\beta_j = |F_{Gr}|^2 / |F_j|^2 \tag{S15}$$

Here index μ refers to a time series of measurements at $t = t_\mu$. Since eq. S13 holds at any time, we can require that coefficients β_j globally minimize deviations from unity, so that

$$\delta\left(\sum_{\mu}\left(1-\sum_{j}\beta_j u_{j\mu}\right)^2\right)=0 \quad . \tag{S16}$$

Using the calculus of variations, it is easy to show that optimum coefficients β_j are given by the solution of a matrix equation

$$\sum_{j}\left(\sum_{\mu}u_{j\mu}u_{j\mu}\right)\beta_j=\sum_{\mu}u_{i\mu} \tag{S17}$$

and the scattering factors for each phase can be obtained from these coefficients using eq. S15. While this approach would yield the most internally consistent estimates for F_j and x_j, we used the independently estimated scattering factors from Table S2 to reduce uncertainty of the analysis even though it means deviations from the optimum given by eq. S16.

Supporting Tables

Table S1. Materials and properties.

Negative electrode (Gr)	91.8 %wt graphite (CGP-A12, ConocoPhillips) 2 wt% C45 conductive carbon (Timcal) 0.17 wt% oxalic acid 6 wt% PVdF binder (KF9300, Kureha) Current collector: 10 μm battery grade Cu 13.5 mg/cm^2 graphite areal density 5.02 mAh/cm^2 graphite areal capacity Coating thickness: 114 μm after calendering Porosity: 38%
Positive electrode (NCM523)	90 wt% NCM523 (Toda Inc.) 5 wt% C45 carbon (Timcal) 5 wt% PVdF binder (Solef 5130, Solvay Inc.) Current collector: 20 μm battery grade Al 20.4 mg/cm^2 oxide areal density 5.66 mAh/cm^2 oxide areal capacity Coating thickness: 111 μm, no calendering Porosity: 47.4%
Microporous separator	Celgard 2325 (PP/PE/PP) Thickness: 25 μm Porosity: 39%
Liquid electrolyte	40 μL 1.2 M $LiPF_6$ in 3:7 w/w ethylene carbonate/ethyl methyl carbonate (Tomiyama Inc., Japan)

Table S2.

Estimated X-ray diffraction scattering factors per unit cell of selected Li_xC_6 species using VESTA software[1] and crystal structures obtained from cited references.

Species	Strongest Bragg peak, (hkl)	Multiplicity m_{hkl}	Estimated F_{hkl}	Value of f_i	reference
graphite	(002)	2	16.8	0	[2]
LiC_{30}	(004)	2	49.72	1/5	[3]
LiC_{18}	(004)	2	33.85	1/3	[3]
LiC_{12}	(002)	2	50.2	1/2	[4]
LiC_6	(001)	2	25.3	1	[4, 5]

[1] K. Momma, F. Izumi, *J. Appl. Cryst.* **2011**, *44*, 1272.

[2] P. Trucano, R. Chen, *Nature* **1975**, *258*, 136; N. S. Nazer, V. A. Yartys, T. Azib, M. Latroche, F. Cuevas, S. Forseth, P. J. S. Vie, R. V. Denys, M. H. Sørby, B. C. Hauback, L. Arnberg, P. F. Henry, *J. Power Sources* **2016**, *326*, 93.

[3] A. Missyul, I. Bolshakov, R. Shpanchenko, *Powder Diffr.* **2017**, *32*, S56.

[4] B. Vadlamani, K. An, M. Jagannathan, K. S. R. Chandran, *J. Electrochem. Soc.* **2014**, *161*, A1731.

[5] L. Boulet-Roblin, P. Borel, D. Sheptyakov, C. Tessier, P. Novák, C. Villevieille, *J. Phys. Chem. C* **2016**, *120*, 17268.

Table S3.

Cell voltage and Li content of layers L_0 to L_4 (Figure 1) in atoms per C_6 unit of graphite as a function of the specific capacity of the graphite electrode during cycling of the cell at 1C rate.

	Specific capacity ($mAh/g_{graphite}$)	Cell Voltage (V)	Layer average x in Li_xC_6				
			L_0	L_1	L_2	L_3	L_4
Layer centroids z_l, μm [a]			8.03	29.0	54.0	79.0	102.6
Charge	8.1	3.56	0.05	0.04	0.04	0.05	0.04
	66.9	3.83	0.21	0.16	0.15	0.16	0.15
	96.4	3.92	0.36	0.30	0.22	0.23	0.21
	125.8	4.03	0.42	0.38	0.36	0.33	0.32
	174.7	4.26	0.66	0.49	0.46	0.45	0.44
	214.1	4.40	0.83	0.63	0.53	0.50	0.49
Discharge	231.8	4.16	0.84	0.74	0.63	0.58	0.56
	192.4	3.91	0.71	0.69	0.61	0.57	0.55
	153.5	3.68	0.44	0.59	0.59	0.56	0.55
	124.1	3.53	0.25	0.40	0.52	0.55	0.55
	104.1	3.45	0.12	0.30	0.40	0.48	0.51
	84.7	3.38	0.08	0.17	0.28	0.37	0.42
	65.2	3.31	0.06	0.09	0.14	0.22	0.25
	35.8	3.08	0.04	0.05	0.05	0.05	0.06
	6.3	3.00	0.02	0.02	0.02	0.02	0.02

a) see eq. S3 in section S1.

Supporting Figures.

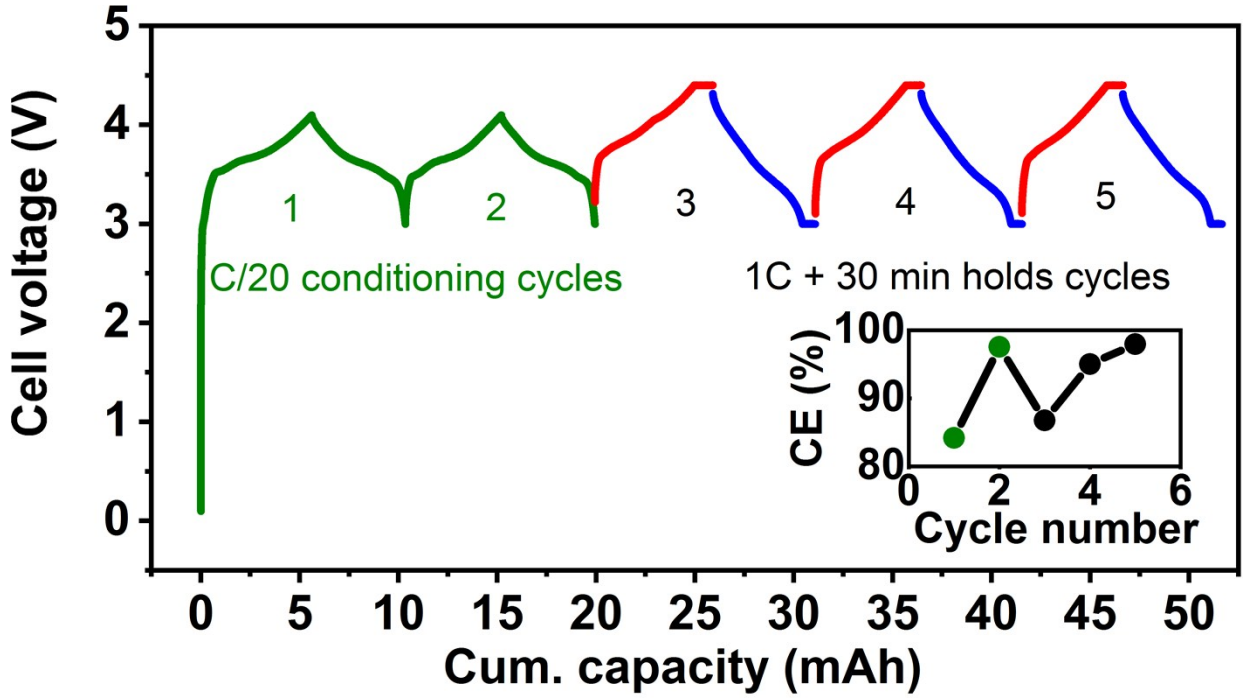

Figure S1. Cycling history of the Gr/NCM523 cell. Cycles 1 and 2 (*shown in green*) are two conditioning cycles carried out at a ~C/20 rate and used to develop a stable SEI layer on the graphite electrode. These cycles were followed by three 1C cycles during which the cell was examined using EDXRD. In the main text we detail only data for cycle 5, whereas in this Supplement we also show the data for cycles 3, 4 and 5 (Figures S2 and S4). The inset shows the coulombic efficiency (CE) of the cell as a function of the cycle number. During the first formation cycle, the CE is considerably less than 100% due to formation of the SEI that traps lithium ions; for the fifth cycle, the CE is approximately 98%.

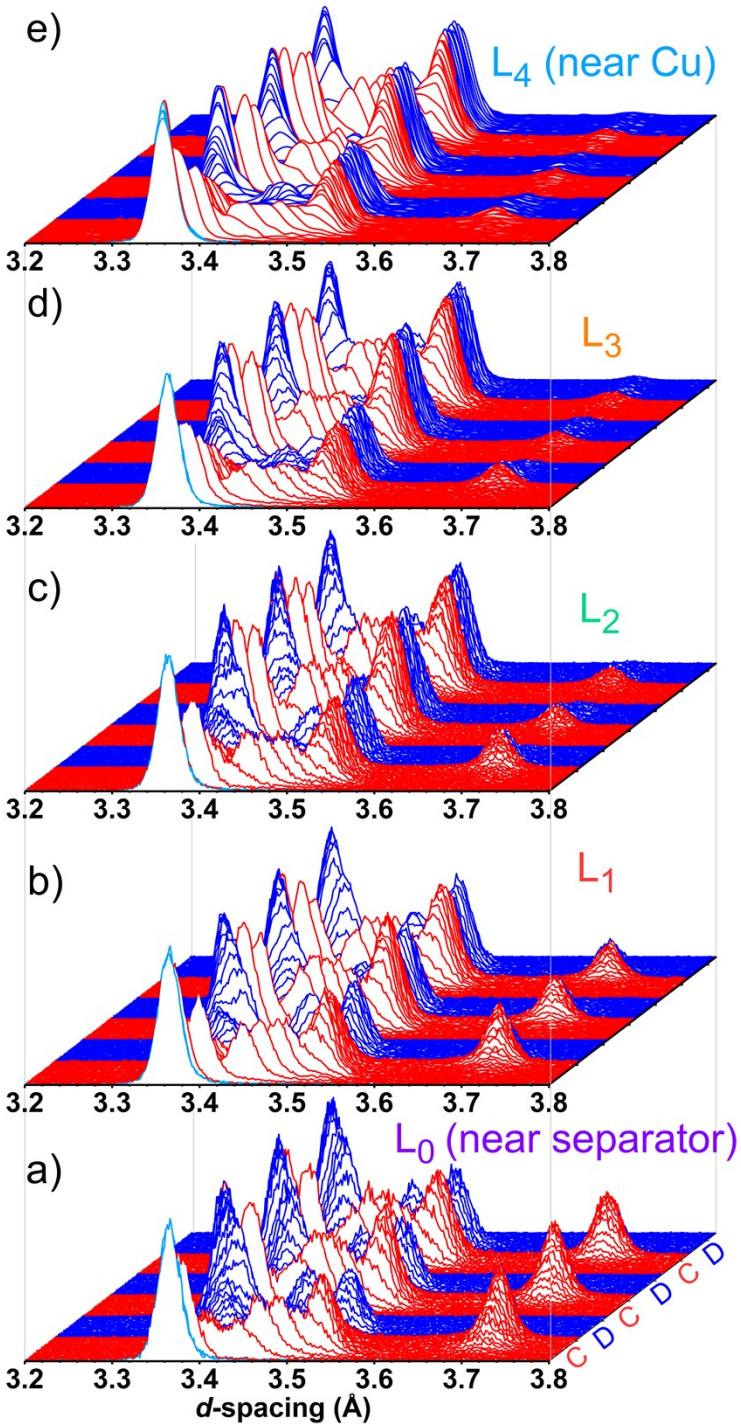

Figure S2. Like Figure 3, for cycles 3 to 5 (see panel a). The axis along the line of sight indicates time. Labels “C" and “D” indicate charge (*in red*) and discharge (*in blue*) of the cell, respectively.

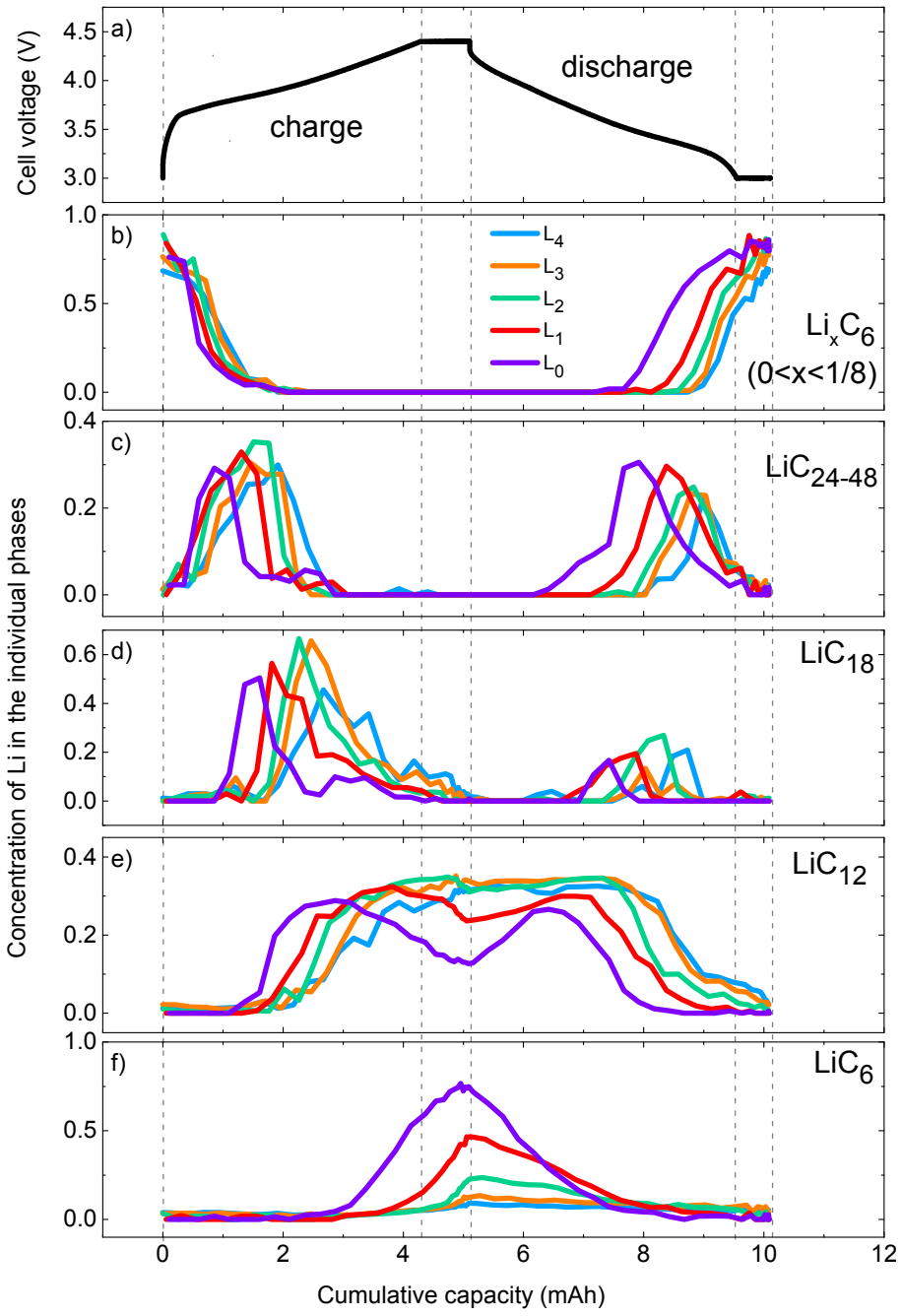

Figure S3. Cell voltage (a) and Li content of the individual Li_xC_6 phases (indicated to the right of panels b to f), plotted as a function of the cumulative capacity for cycle 5 in Figure S1. The color coding of layers L_0 to L_4 corresponds to Figure 1 in the main text and it is repeated in panel b.

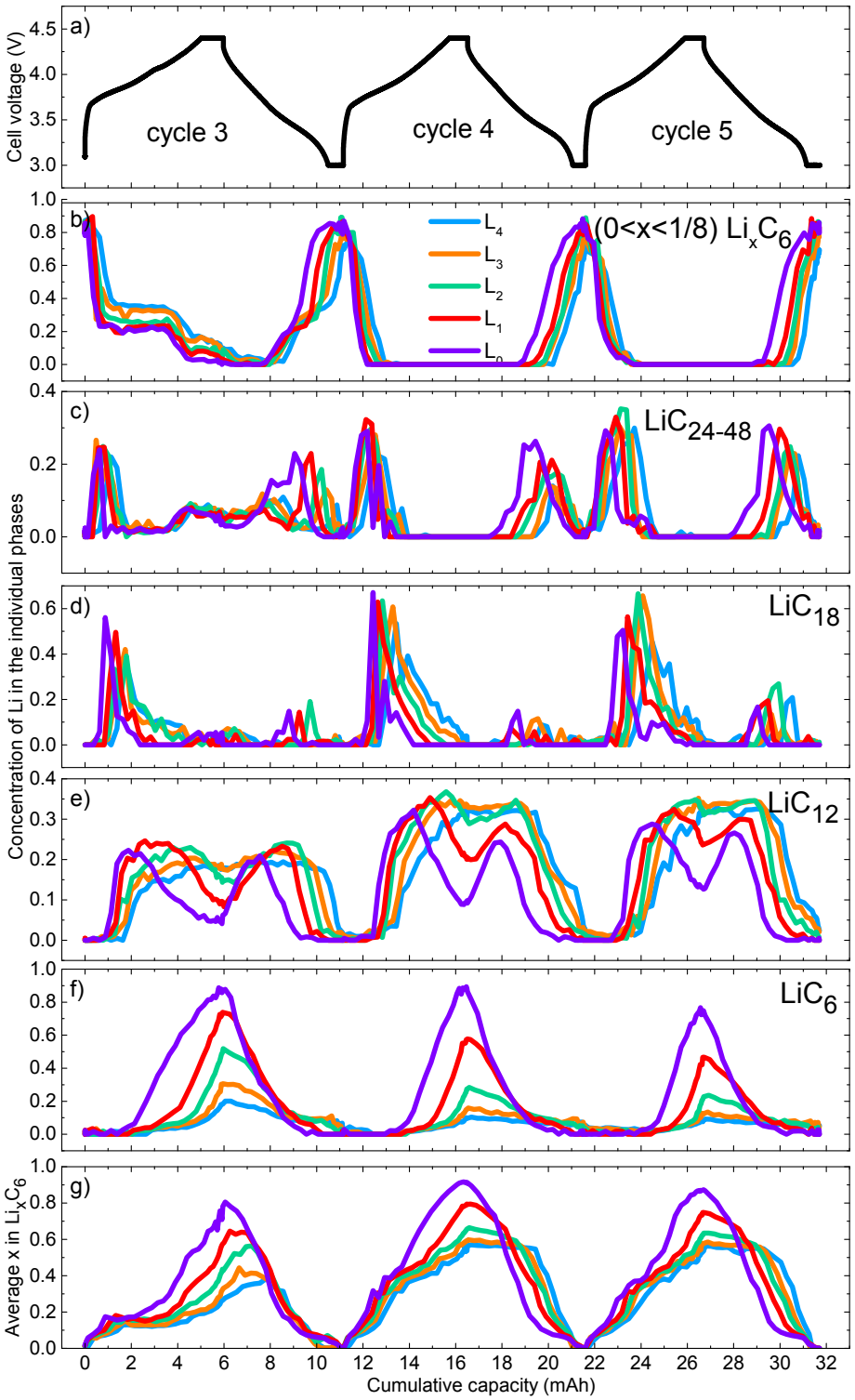

Figure S4. Li content of the individual Li_xC_6 phases for cycles 3, 4, and 5 (see panel a) is shown in panels b to f. In panel g, the layer average Li content *x* is shown.

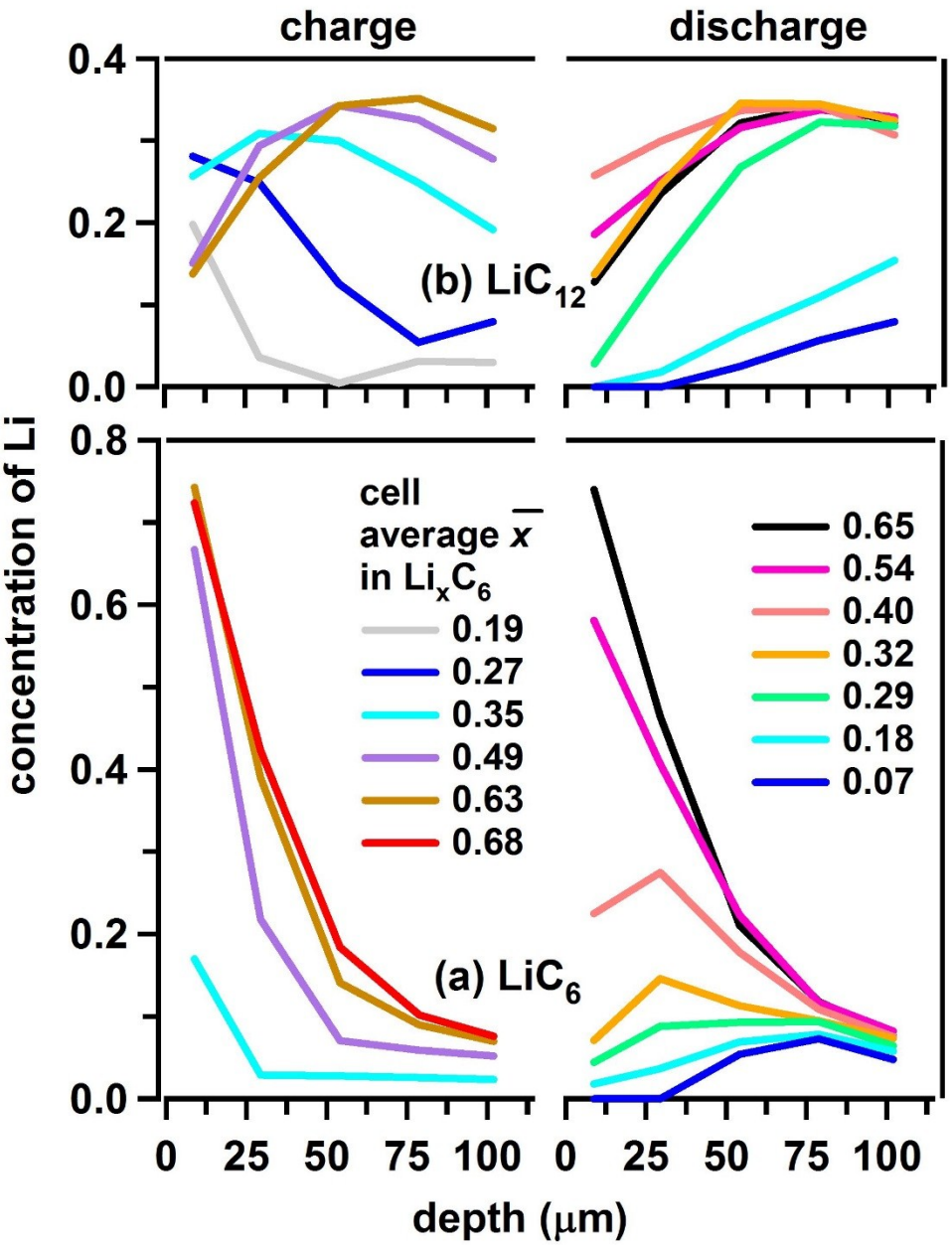

Figure S5. The *layer* average Li content in (a) LiC_6 and (b) LiC_{12} phases plotted vs. the median depth z of the five layers shown in Figure 1 in the text. The *cell* average Li content during 1C cycling of the cell is indicated in the plot. The curves on the left correspond to charging of the cell, and the curves on the right correspond to discharging of the cell. The color lines are straight segments connecting the data points.

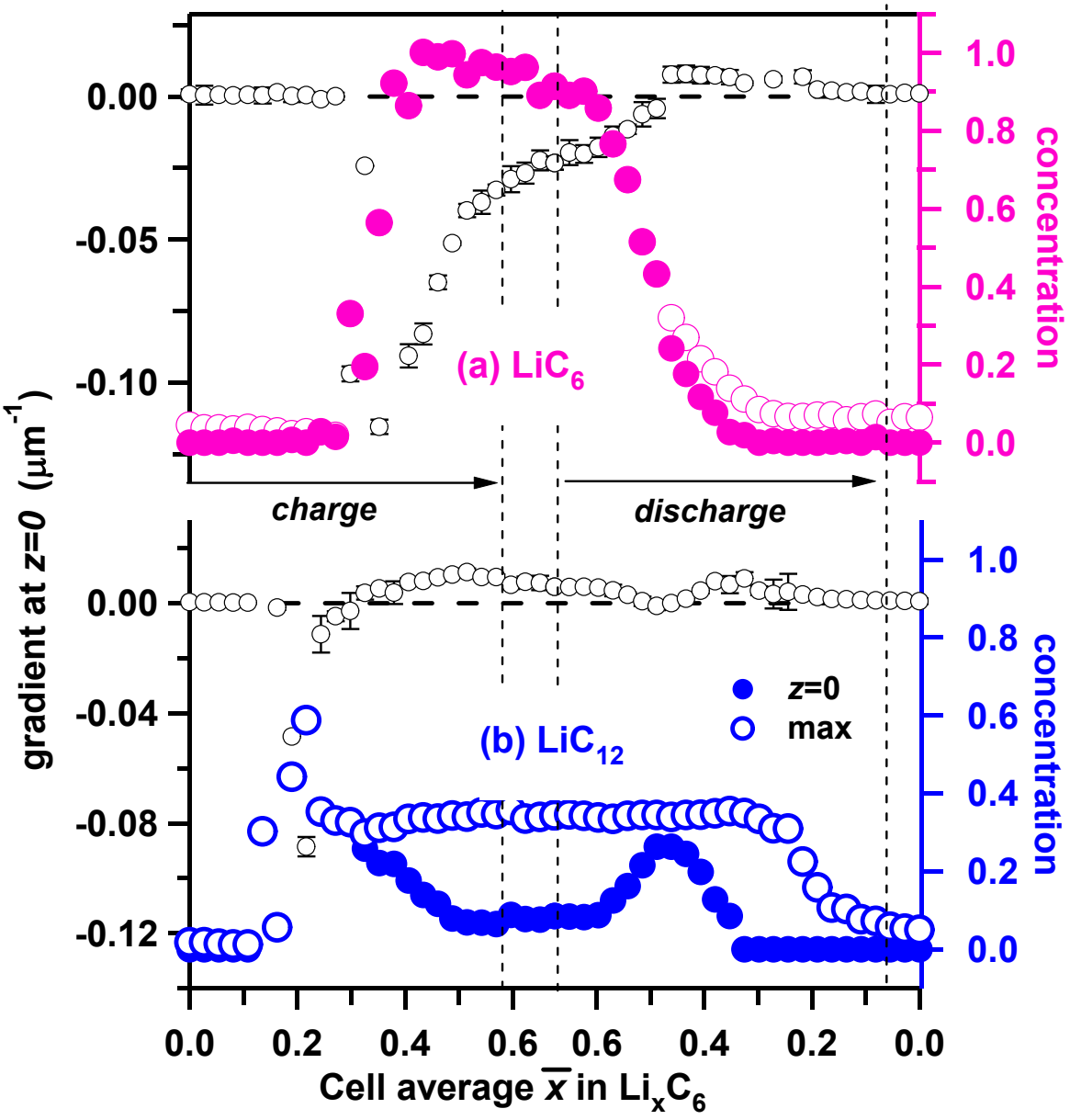

Figure S6. Like Figure 10 in the text with the error bars for the gradients determined from the nonlinear least squares fit procedure explained in section S1.

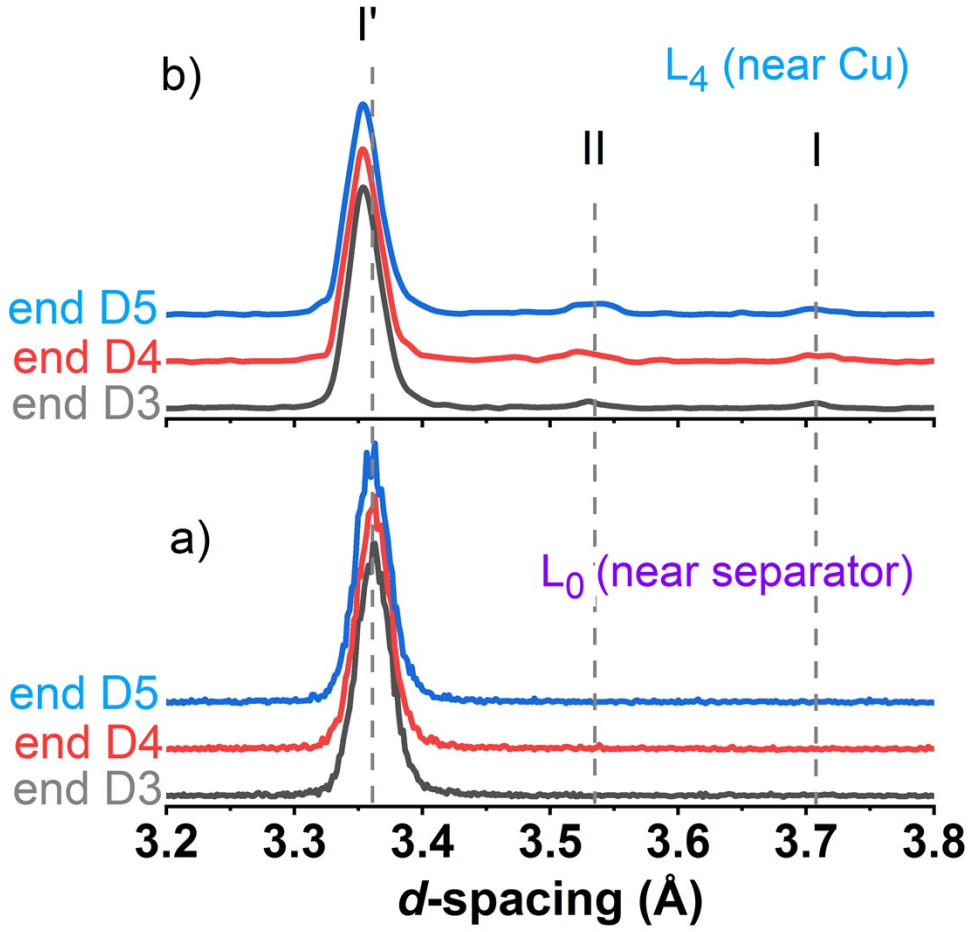

Figure S7. Evidence for residual lithiated stages I and II (LiC_6 and LiC_{12} phases, respectively) at the end of 1C discharge followed by a 30 min potentiostatic hold at 3 V. X-ray diffraction patterns for cycles 3 (D3), 4 (D4), and 5 (D5) in Figure S1 are shown in each panel. It is seen that near the electrode surface (layer L_0 in panel a) the removal of LiC_6 and LiC_{12} is complete, while at the back of the electrode near the current collector (layer L_4 in panel b) it is incomplete. This residual Li can be partly responsible for the coulombic efficiency of 98% seen in the inset of Figure S1.

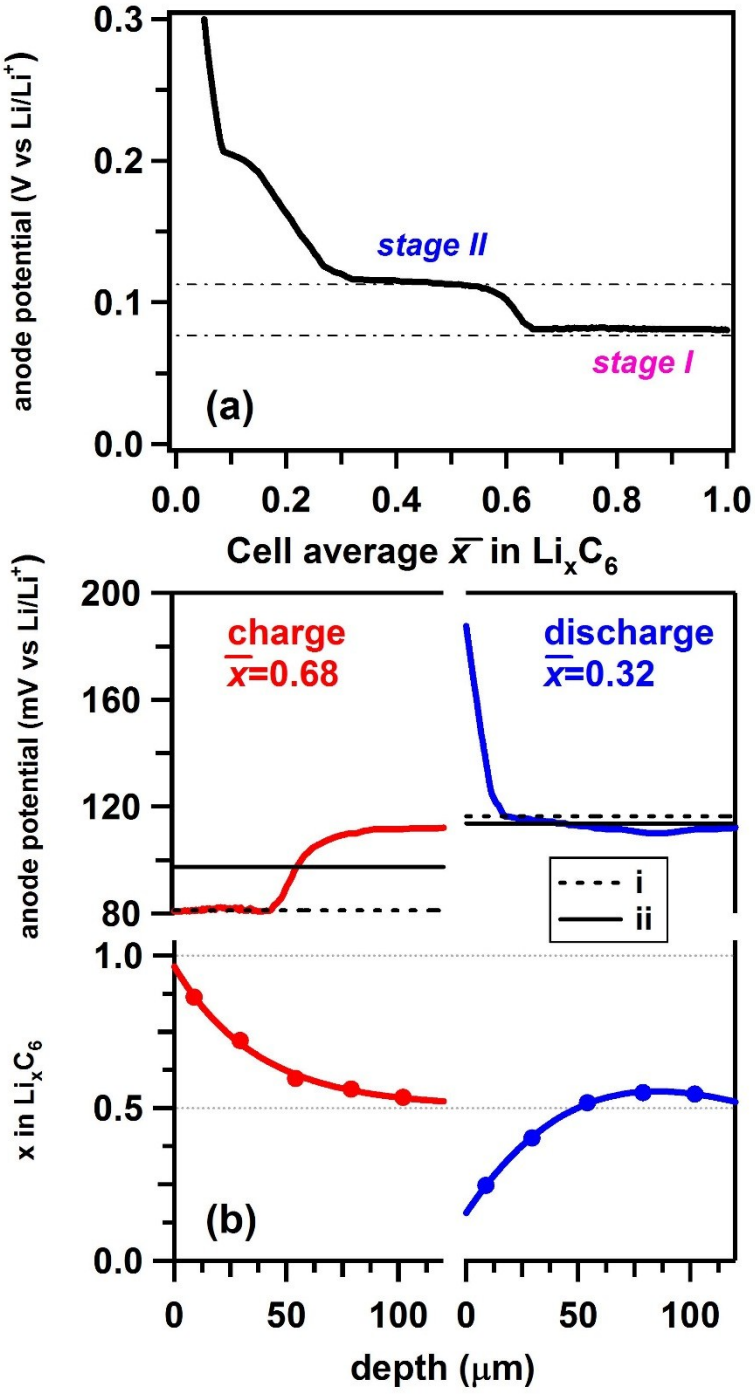

Figure S8. (a) Anode potential in Gr/NCM523 cell equipped with a lithiated copper wire reference electrode (C/25 cycling). (b) Transformation of two Li concentration profiles from Figure 8 (with the state of charge indicated in the plot) to the fictitious anode potential profiles using the plot in panel a. The horizontal dashed black lines (i) indicate the potential in panel a that corresponds to the cell average Li content, while the solid black line indicates the cell average potential. At the peak charge (*on the left*) the two potentials differ by ≈ 17 mV.